This is the accepted manuscript of Thygesen, L. G., Beck, G., Nagy, N. E., & Alfredsen, G. (2021).
Cell wall changes during brown rot degradation of furfurylated and acetylated wood. International Biodeterioration & Biodegradation, 162, 105257.
The version of record can be accessed at http://dx.doi.org/10.1016/j.ibiod.2021.105257

Cell wall changes during brown rot degradation of furfurylated and acetylated wood

Lisbeth G. Thygesen[a]*, Greeley Beck[b], Nina E. Nagy[b] and Gry Alfredsen[b]

[a] *Department of Geosciences and Natural Resource Management, University of Copenhagen, Rolighedsvej 23, 1958 Frederiksberg C, Denmark*

[b] *Norwegian Institute of Bioeconomy Research (NIBIO), P.O. Box 115, NO-1431 Ås,*

**Corresponding author.*

Key words: acetylation, brown rot decay, furfurylation, *Rhodonia placenta*, light microscopy, Attenuated Total Reflectance Fourier Transform InfraRed (ATR-FTIR) spectroscopy, Raman microspectroscopy, Confocal Laser Scanning fluorescence Microscopy (CLSM)

Abstract

This study explores cell wall changes in Radiata pine (*Pinus radiata*) after modification with acetylation or furfurylation and subsequent prolonged subjection to the brown rot fungus *R. placenta* with the aim of better understanding the *modus operandi* of these two modifications. Both modifications have shown good durability in field tests, but in order to learn from their possible limitations, we used optimal environmental conditions for fungal growth, and extended the testing period compared to standard tests. Hyphae were found in acetylated wood after two weeks, and after 28 weeks of decay abundant amounts of encapsulated hyphae were present. In furfurylated wood, mass loss and a few hyphae were seen initially, but no further development was seen during weeks 18-42. The general degradation pattern was qualitatively the same for unmodified, acetylated and furfurylated wood: carbohydrates decreased relative to lignin. Acetyl groups were lost from acetylated wood during decay (earlier results), while the furan polymer did not seem to be altered by the fungus. Based on these findings it is hypothesized that modifications such as furfurylation that enhance moisture exclusion within the cell wall through impregnation polymerization offer better long term protection compared to modifications such as acetylation that depend on the replacement of hydroxyl groups with ether bound adducts that can be removed by fungi.

1. Introduction

Fungi are important decomposers of woody biomass in natural habitats. For wooden building materials, long, predictable service life and carbon storage are however essential, making prevention of fungal decay pivotal to any use of wood or wood-based materials for construction purposes. One of the avenues followed is wood modification, as it provides dimensional stability and extends the service life of wood by protecting it from biological attack without the use of biocides. The three main commercialized wood modification processes (acetylation, thermal modification, furfurylation), have gained market shares in Europe across a wide range of use classes (Sandberg, et al., 2017). This development has been possible because the methods have been tested extensively and much is already known about their performance in practice and in standard tests. However, further development of wood modification processes is at present hampered by a lack of knowledge on the details of how and why the methods used so far prevent or delay fungal decomposition, albeit it has been established that a reduction in moisture content is involved (Thybring, 2013; Thybring et al., 2018). In the current study, we explore the cell wall changes in *Pinus radiata* after modification with acetylation or furfurylation and subsequent subjection to a brown rot fungus to understand the *modus operandi* of these two different modifications better.

Acetylation implies impregnation with acetic anhydride, which then reacts with hydroxyl groups in the wood cell wall in a nucleophilic substitution reaction replacing hydroxyls with acetyl groups (Fuchs, 1928). Furfurylation, on the other hand, is a process where wood is impregnated with furfuryl alcohol, which then polymerizes within the wood cell wall during the following curing step (Westin, 2004). It is likely that cross-linking to cell wall lignin to some extent also takes place, but not via hydroxyl groups (Nordstierna et al., 2008; Barsberg and Thygesen, 2017). This implies that both methods bulk the cell wall, i.e reduce the space available for cell wall water, but only acetylation directly consumes hydroxyl groups otherwise available for hydrogen bonding to water molecules.

A large part of the biological deterioration of timber in service is due to the action of brown rot fungi (Arantes and Goodell, 2014). The mechanisms of brown rot degradation of wood have been reviewed by e.g. Arantes and Goodell (2014) and Goodell et al. (2020). Briefly summarised ”Fungi that cause brown rot depolymerize cellulose and hemicellulose (holocellulose) for digestion, while lignin is also depolymerized and modified before being rapidly repolymerized” (Goodell et al. 2020). Characterization of the chemical changes of the wood material during brown rot degradation have been described in Curling et al., 2002; Irbe et al. 2006, 2011; Fackler et al., 2010, Winandy and Morrell, 1993; Winandy, 2016, 2017.

Studies profiling chemical composition during different stages of brown rot of modified wood are scarce or only evaluate one stage of decay (e.g. Clausen and Kartal, 2003, Ehmcke et al., 2020).

It was recently found that given optimal conditions for fungal decay and prolonged exposure time, brown rot fungi may deacetylate acetylated *Pinus radiata*, and then proceed to degrading the cell walls (Beck et al., 2018a). Under the same experimental conditions, furfurylated *P. radiata* appears initially to be slightly degraded, but then degradation halts (Skrede et al., 2019). Although both modifications delayed degradation, late harvest times for highly acetylated samples showed high relative gene expression for core plant cell wall-hydrolyzing enzymes whereas furfurylated samples generally showed downregulation of such enzymes after longer incubation times (Beck et al., 2018b; Skrede et al., 2019). This indicates that once degradation begins in the two modified materials, the fungus employs different degradation strategies with differing degrees of success. This study further explores brown rot degradation of furfurylated and acetylated wood by examining aspects of cell wall chemistries in the two cases with the aim of identifying modification and/or degradation patterns that covaried with the two dissimilar trends. Wood samples of both modification types were analyzed before and after brown rot degradation using light microscopy and infrared spectroscopy. To obtain additional spatially resolved information, acetylated samples were analyzed using Raman microspectroscopy, while furufylated samples were analyzed using Confocal Laser Scanning fluorescence Microscopy (CLSM). Raman spectroscopy can identify the location of acetyl groups via the signal from their carbonyl moieties. This is because unmodified wood only has a very weak Raman band for carbonyl, i.e. the signal can safely be ascribed to the modification. This is in contrast to infrared spectroscopy, which is more sensitive to carbonyl groups. Consequently, also carbonyl groups in unmodified wood are detected using this method. Furfurylated wood cannot be analyzed using Raman spectroscopy due to autofluorescence from the modification. However, fluorescence spectroscopy and CLSM can be used to characterize the furan polymer (Thygesen et al., 2010a, 2020).

The hypothesis of the current study was that bulking of the wood cell wall is the common mechanism in wood protection against brown rot fungi for both modification methods studied, and that the bonding of acetyl groups to the wood cell wall hydroxyl groups only provides transitory protection to acetylated wood.

2. Materials and methods

2.1 Wood material

A *Pinus radiata* (D. Don) sapwood board was initially cut in the transverse plane to produce 10 mm thick slices. As described in Beck et al. (2017), cylinders 6 mm in diameter were then punched out of the earlywood portion of the growth rings with a steel hole punch so that the cylinder length was oriented along the fiber direction. Before treatment, all samples were dried at 103°C for 18 h and then cooled in a desiccator before the initial dry weight was recorded.

Radiata pine is the most frequently used wood material for both the furfurylation and the acetylation process because it is easy to treat. We chose to use only earlywood in order to make the samples as homogeneous as possible.

2.2 Treatments

Furfurylation: Synthesis grade 98% furfuryl alcohol (Merck, Darmstadt, Germany) was used according to the formula by the company Kebony AS, with a furfuryl alcohol-to-water ratio of 7:10 (commercial treatment level). The samples were soaked in the furfuryl alcohol solutions for 15 days. Sets of five samples were wrapped in aluminum foil and cured at 120°C for 16.5 h.

Acetylation: Acetylation procedures are described in detail in Beck et al. (2018a). The samples were impregnated with acetic anhydride (Merck, Darmstadt, Germany) and acetylated at 110°C for 1750 min.

After treatment, both modified and unmodified control samples were leached according to EN 84 (CEN 1997) and dried at room temperature. In order to provide data for weight percent gain (WPG) and initial dry mass after treatment, the samples were dried at 103°C for 18 h and then cooled in a desiccator before the dry weight was recorded. Outliers with high or low WPG were excluded from the material after treatment and before the decay tests. The remaining samples were randomly distributed throughout the test. The recorded mean weight percent gain (WPG) was 36.1±5.5% for furfurylated samples and 21.4±0.7% for acetylated samples. Then the samples were left in a climate chamber at 65% relative humidity and 20°C until stable weight before they were sealed in plastic bags and sterilized by gamma irradiation (25 kilogray [kGy]) at the Norwegian Institute for Energy Technology.

2.3 Decay test

Since we needed a prolonged incubation time, the traditional malt-agar medium could not be used because the medium would dry out. The malt-agar medium also adds large amounts of readily available sugar into the test system. Therefore, a test system with sterile soil and inoculation with liquid culture was used, as it has proven to work well for prolonged incubation

periods. After determining the initial weights of the Petri dishes (plates), sterile water can be added every third week to make sure the soil does not dry out. In this experiment the specimens were exposed to *Rhodonia placenta* (Fr.) Niemelä, K.H. Larss. & Schigel (syn. *Postia placenta*) strain FPRL 280 (BAM113). The fungus was first grown on 4% Difco malt agar medium (VWR) and plugs from actively growing mycelia were transferred to a liquid culture containing 4% Difco malt (VWR). After 2 weeks, the liquid culture was homogenized with a tissue homogenizer (Ultra-Turrax T25; IKA Werke GmbH & Co. KG, Staufen, Germany). Soil (2/3 compost soil and 1/3 sandy soil) was adjusted to 95% of the soils water-holding capacity according to ENV 807 (CEN 2001). In each Petri dish (TC dish 100, standard, 87 mm diameter, 20 mm, Sarstedt AG & Co., Nümbrecht, Germany) 20 g sterile soil was added, and a plastic mesh was used to avoid direct contact between the wood samples and the soil. A 300 µl inoculum of homogenized liquid culture was added to each specimen. Eight wood samples of the same treatment were added to each plate, and four replicate plates were used. Samples were incubated at 22°C and 70% RH and harvested every third week in experiments with furfurylated wood (42 weeks in total), every second week in experiments with acetylated wood (28 weeks in total), and every week for the unmodified wood material (5 weeks in total). The weights of all plates were measured at all harvest points and sterile water was added when needed in order to keep the moisture conditions stable. After harvest, fungal mycelium was manually removed from the wood surface with delicate task wipes (Kimtech Science, UK) in order to obtain fungal mass for the wood mass loss measures. Eight samples from each treatment and each harvesting point were dried at 103°C for 18 h in order to provide data for mass loss. The remaining samples were wrapped individually in aluminum foil and put directly into a container with liquid nitrogen, then stored at -80°C. From the furfurylation experiment RNA-seq transcriptome data is reported in Skrede et al. (2019) and accessibility of hydroxyl groups reported in Beck et al. (2019). Low-field NMR, hydroxyl accessibility and acetyl content data from the acetylation experiment is reported in Beck et al. (2018a) and qRT-PCR transcriptome data in Beck et al. (2018b).

2.4 Light microscopy

The fungal degradation experiment performed on wood blocks used for microscopy analyses included: 1) unmodified material prior to fungal incubation (0) and after 4 weeks of incubation, 2) acetylated wood prior to fungal incubation (0) and after 2 and 28 weeks of incubation, 3) furfurylated wood prior to fungal incubation (0) and after 3 and 42 weeks of incubation. Each block was cut in half, and 5 mm-wide specimens of the central core were fixed in paraformaldehyde (2%) and glutaraldehyde (1.25%) in Pipes buffer (50 mM, pH 7.2) for 12 h at room temperature. The wood blocks were embedded in LR White resin (Electron Microscopy Sciences, Hatfield, PA, USA) and 2 µm-thick cross sections were cut using a Leica Ultra-

Microtome EM UC6 (Leica Microsystems). To visualize the effect of treatments and hyphae growth inside the samples, the preparations were stained with a mixture of 2% potassium permanganate and 1.3% methylene blue (del Cerro et al., 1980). This stain gives a general staining of all cell components including cell wall lignin, pectic substances and phenols. Periodic acid-Schiff (PAS) Kit (Sigma, St. Louis, MO, USA) was used for staining cell wall structures containing a high proportion of carbohydrate-rich compounds following a protocol described by Feder and O'Brien (1968) with minor modifications. Slides were placed in periodic acid (0.5%) for 30 mins, rinsed with MQ water, and placed in Shiff's reagent for 30 minutes in darkness and were then rinsed with MQ, dried and mounted. Total carbohydrates of insoluble polysaccharides stain magenta to purplish red. Images were taken with bright field optics using a Leica DMR light microscope.

2.5 Attenuated total reflectance Fourier transform infrared (ATR-FTIR) spectroscopy

Attenuated total reflectance Fourier transform infrared (ATR-FTIR) spectroscopy was used to chemically characterize the materials. The data for acetylated and unmodified samples was originally reported in Beck et al. (2018a) but is reanalyzed and presented together with furfurylated samples in the current study. Acetylated and unmodified samples were oven dried for 18 h at 103°C to determine mass loss for each wood specimen individually. The dried specimens were then ball-milled using a Retsch 300 mill (Retsch mbH, Haan, Germany) with a 100 mg stainless steel bead (QIAGEN, Hilden, Germany) at maximum speed for 1.5 min. The powdered samples were used for the FTIR measurement. Three replicate spectra were obtained for each sample and three samples were used for each harvest time. The harvest times for unmodified samples were 0, 1, 2, 3 and 4 weeks while the harvest times for acetylated samples were 0, 10, 16, 24 and 28 weeks. A Bruker Tensor 27 FTIR with platinum ATR accessory (Bruker, Billerica, MA, USA) was used to perform the FTIR measurement for the acetylated and unmodified samples. 64 scans were obtained (128 for background) using a resolution of 4 cm^{-1} and a spectral range of 4000-600 cm^{-1}.

For the furfurylated samples, a single specimen from each harvest time (0-42 weeks, every third week) was analyzed with FTIR. The frozen samples were thawed, and a razor blade was used to split the sample vertically. Five small pieces were then shaved from the interior of the sample and the pieces were dried at 60°C overnight. The samples were then stored at ambient conditions similar to the conditions during FTIR measurements for at least 2 weeks. A Nicolet 6700 FT-IR spectrometer (Thermo Scientific, Waltham, MA, USA), equipped with a Pike Technologies GladiATR diamond ATR was used for the FTIR measurements for the furfurylated samples. The same measurement settings were used as those for the acetylated and unmodified samples.

All spectra were analyzed using Rstudio (Rstudio Team, Boston, MA, USA). First, the spectral range between 2800-1900 cm^{-1} containing no information on the wood samples was removed and then the spectra were baseline corrected using the "hyperspec" package (Beleites et al., 2020). The rubberband baseline correction method was used with 20 degrees of freedom and a noise level of 0.003. Partial least squares regression was performed on the FTIR spectra to obtain models for mass loss using the "pls" package (Mevik et al., 2020). Mass loss data was used for the individual specimens from which the unmodified and acetylated powdered replicates were obtained. Because individual mass loss data was unavailable for the furfurylated samples, the average mass loss obtained at each harvest point (Fig. 1) was used instead. Three models were obtained, one for each treatment. Analysis of the root mean square error of cross validation revealed that three components were sufficient for each model. Full cross validation was used, i.e. spectra from all replicates of a given sample were left out of the calibration in each step of the cross validation.

2.6 Confocal Laser Scanning fluorescence Microscopy (CLSM)

Furfurylated wood cannot be analyzed using Raman spectroscopy due to autofluorescence. Consequently, Confocal Laser Scanning fluorescence Microscopy (CLSM) was used to characterize the furan polymer (Thygesen et al., 2010a, 2020). The samples were analyzed using CLSM (before and after 42 weeks of incubation). Images were acquired from cross sections. The instrument used was a confocal laser-scanning microscope (SP5-X, Leica Microsystems, Wetzlar, Germany) equipped with a tunable white light laser and a 63x objective (water immersion). The same gain settings were used throughout, thus allowing direct comparison of emission intensities obtained using the same excitation wavelength. Three different data sets were obtained per location: 1) emission in the 500-600 nm range after excitation at 488 nm, 2) emission in the 650-700 nm range after excitation at 633 nm and 3) 4-way data in the form of fluorescence landscapes obtained for each image pixel. Each landscape consisted of 21 excitation steps between 470 and 670 nm (i.e. step size 10 nm) and 23 20 nm wide emission steps in the range from 490 to 710 nm (step size 10 nm). Only wavelength combinations where emission wavelength was longer than excitation wavelength were included. For 1) and 2) images were obtained as 1024 x 1024 pixels using averages of sixteen scans to reduce noise, for 3) as 512 x 512 pixels using averages of 8 scans. In all cases, images measured 82.01 x 82.01 µm (3x zoom applied), i.e. the pixel size was either 80.17 x 80.17 nm (data types 1 and 2)or 160.49 x 160.49 nm (data type 3). For all data types, three images/data sets were captured from the furfurylated wood both before and after fungal degradation, i.e. in total data from six regions were obtained.

Type 3) data were analyzed in Matlab ver. R2017b (Mathworks, Natick, Massachusetts, USA). Multivariate Curve Resolution – Alternating Least Squares (MCR-ALS) modelling was performed on each of the CLSM images in order to obtain spectral signals from the different chemical components present in the wood sections. The Matlab GUI 2.0 by Jaumot et al. (2015) was used to model the unfolded image matrix, and non-negativity constraint was enforced in both directions of the model. Due to hardware limitations, the number of pixels was reduced to 171 x 171 before analysis. After evaluating the suitable number of components using Singular Value Decomposition, the number of components was set to three for all images.

2.7 Raman microspectroscopy

Only acetylated samples were analysed using Raman Microscopy (furfurylated wood causes autofluorescence). Raman images were acquired from cross sections with a confocal Raman microscope (WITec alpha300R, WITec GmbH, Ulm, Germany) equipped with a UHTS 300 spectrometer and a 100x oil immersion objective (NA = 1.4). A linear polarized 532-nm NdYag laser was focused with a diffraction limited spot size of $0.61 \times \lambda/NA$ resulting in a spectral resolution of 0.3 µm. The intensity was 20 mW prior to the objective and the acquisition time for each spectrum was 0.1 second. Raman light was detected with an air cooled back-illuminated charge-coupled device (CCD) detector in the spectral range from 100 to 1800 cm^{-1} with a spectral resolution of 6 cm^{-1}. The xylem micro sections were aligned under the microscope with the tangential direction parallel to the laser polarisation (Gierlinger et al., 2012). The software WITec Control 5.06 was used for spectral acquisition. Three images were obtained from the acetylated wood both before and after fungal degradation (28 weeks), i.e. in total six images.

Raman data were analyzed in Matlab ver. R2017b (Mathworks, Natick, Massachusetts, USA). Prior to analysis spectra were subjected to 1) removal of the lower part of the spectrum not used in the analysis (wavenumbers below approximately 1200 cm^{-1}), 2) cosmic ray removal by use of median filtering (Matlab build-in function medfilt1 using default settings), 3) Alternating Least Squares (ALS) base line correction according to Eilers and Boelens (2005) with parameters $\lambda=10^9$, p=0.001 and the number of iterations set to 10, and 4) Savitzky-Golay smoothing using a 7-point moving window and a 3rd degree polynomial (PLS Toolbox for Matlab, version 8.02 from Eigenvector Research Inc., Manson, Washington, USA). Each image was subjected to kmeans cluster analysis (as implemented in Matlab) using two clusters, which successfully separated cell wall from lumina and intercellular spaces. For the spectra assigned to cell wall, Raman peak areas were estimated by use of Trapezoidal numerical integration (Matlab trapz function) and using a linear baseline, individually set for

each Raman band. The peak areas estimated were: 1) aromatic ring stretching at 1601 cm^{-1} (Gierlinger and Schwanninger, 2007), area calculated for the range 1580-1650 cm^{-1} and assigned to lignin, 2) Carbonyl stretch at 1732 cm^{-1} (Marchessault and Liang, 1962), area calculated for the range 1700-1750 cm^{-1} and assigned to acetylation and 3) CH and CH_2 stretching in the 2900 cm^{-1} region (Wiley and Atalla, 1987), area calculated for the range 2800-3050 cm^{-1} and assigned to cell wall material. The cell wall spectra were further sorted into S2 layer vs. middle lamella and cell corners by use of the peak area ratio between the lignin and the cell wall material peak areas, i.e. spectra with a ratio above 0.2 were assigned to the latter lignin-rich category. Expressions of acetylation intensity were calculated for each of the two cell wall categories as the ratio between the acetylation signal and either the lignin or the cell wall signal. Fig. SI1 visualizes the Raman data analysis procedure.

3. Results

3.1 Mass loss

When subjected to the brown rot fungus *R. placenta* furfurylated wood was initially degraded , and then degradation stopped/slowed down from week 18 until the end of the experiment, week 42 (Fig. 1). The mass loss data up to 21 weeks was previously reported in Skrede et al. (2019), but the remaining data is reported for the first time in the current study. Acetylated wood initially resisted degradation, and thereafter degradation increased (Fig. 1, as reported earlier by Beck et al., 2018a,b). Acetylated wood had less than 1% mass loss up to week 14, thereafter the rate of degradation accelerated and achieved levels comparable to those of the unmodified samples. However, variation among replicates was high for these late harvest times.

3.2 Location and timing of fungal activity in the wood tissue

Observations of the wood preparations by light microscopy revealed the spatial-temporal degradation patterns in the modified wood, as compared to unmodified wood (Fig. 2).

In unmodified wood, the cell walls of tracheids were after 4 weeks significantly degraded by the fungus and subsequently mass loss was detected (Fig. 2 A, D). The cell walls had an irregularly collapsed shape and hyphae of the fungus were observed in the lumina of the tracheids (Fig. 2D). Also, an effect of the decay was observed in the change in coloration of the cell wall, which appeared darker when comparing Fig. 2A and 2D.

In acetylated wood fungal hyphae were observed in lumina of tracheids after 2 weeks of incubation (Fig. 2B, E). After 28 weeks of incubation (Fig. 2H), representing the end point of the degradation experiment where a mass loss of about 40% was measured (Fig. 1), larger

amounts of hyphae were observed within the cell lumina of both ray cells and tracehids, and many of them showed a thick encapsulation. We used a carbohydrate specific staining (Periodic acid – Schiff's stain), which visualized presence of a polysaccharides in cell walls and fungal hyphae (Fig. 2G, and 2J-L). This staining indicated presence of a hyphal sheath covering the hyphae in unmodified and acetylated wood (Fig. 2J, K).

In furfurylated wood, the tissue at 42 weeks appeared nearly similar to the tissue at 0 and 3 weeks of incubation with the fungus (Fig. 2C, F, I). No fungal hyphae were observed, even after 42 weeks and the integrity of the cell walls seemed to be maintained (Fig. 2I, L). The characteristic yellowish filling seen in some cell lumina is furan polymer (Thygesen et al., 2010a, 2020).

3.3 Bulk chemical changes due to decay

Chemical changes in the bulk material were assessed with ATR-FTIR spectroscopy. Fig. 3A shows average FTIR spectra from all replicates prior to decay and at the end point of the degradation experiment. Fig. 3B shows a closer view of the average spectra for the samples prior to decay. The effect of acetylation is apparent from the increased intensities observed at 1732, 1370 and 1225 cm^{-1} attributed to the C=O valance vibration of acetyl groups, aliphatic C-H stretch in CH3 and C=O stretch in acetyl groups, respectively (Fackler et al., 2010; Faix, 1991; Schwanninger et al., 2004). The changes due to furfurylation were more subtle. An increase in intensity for spectra of furfurylated wood compared to spectra of unmodified wood can be seen at the 1695 cm^{-1} trough, which is assigned to the –HC= linkage in the C=C structure of the furfuryl alcohol polymer (Barsberg and Thygesen, 2009). A slight shoulder is visible at 985 cm^{-1} in the furfurylated spectra and is attributed to –HC=CH– out of plane deformation (Faix, 1991). Both modifications showed decreased intensity in the 3600-2900 cm^{-1} region, broadly assigned to OH stretching vibrations (Fackler et al., 2010).

3.3.1 Partial least squares regression (PLSR) prediction of mass loss based on FTIR spectra

PLSR models of mass loss were used to aid in the interpretation of degradation patterns based on FTIR spectra. The regression coefficients of the models when transformed back to simple regression models based on the spectra are the values used to predict the mass loss from the FTIR prediction matrix and can consequently be used for identifying absorbance bands that change during decay. Wavenumbers in FTIR spectra with large, positive regression coefficients indicate bands for which high absorbance is associated with high mass loss whereas large, negative values are bands negatively correlated to mass loss, i.e. they are associated with low mass loss.

Regression coefficients from the PLSR models are shown in Fig. 4. The magnitude of the regression coefficients reflects the degree of degradation of the samples analyzed. Whereas the maximum mass loss for the individual samples used in the PLSR model for acetylated and unmodified samples was between 50-60%, the furfurylated samples only reached a maximum of 15% mass loss. Thus, regression coefficients for the furfurylated model are much smaller.

Lignin related wavenumbers at 1510 and 1268 cm^{-1} have large positive regression coefficients for the unmodified and acetylated models, while carbohydrate related wavenumbers at 1107 and 1056 cm^{-1} show low values (Fackler et al., 2010; Faix, 1991; Schwanninger et al., 2004). This indicates an increased proportion of lignin in the decayed material and removal of carbohydrates. The model for acetylated wood shows much larger negative values compared to the unmodified model at the acetyl related 1732 cm^{-1} band (Faix, 1991). This suggests a greater reduction in acetyl content in acetylated wood during degradation compared to unmodified wood. The model for furfurylated wood appears to deviate from the other two near the 1695 cm^{-1} band, which has been proposed to be associated with the furfuryl alcohol polymer (Barsberg and Thygesen, 2009). Thus, higher mass losses seem to be related to higher proportions of furfuryl alcohol polymer in the material, suggesting the furfuryl alcohol polymer is unaffected by decay.

3.4 Local chemical changes of decay

As explained in section 1, two different methods where needed to obtain information on the effects of decay on the two modifications at cell and cell wall level.

3.4.1 Effects of decay on acetylated wood cell walls

The results of Raman microspectroscopy of the acetylated wood specimens did not show any systematic differences in the amount or location in acetylation between specimens analyzed before and after fungal decay (Table 1). This contradicts the results from IR spectroscopy (section 3.3) as well as from analysis using saponification of other acetylated wood specimens from the same experimental trial (Beck et al., 2018a) according to which deacetylation took place. An explanation could be that the degraded specimens prepared for Raman microspectroscopy might have been biased towards less degraded regions, as successful microtoming is more likely to happen for these regions than for the more degraded ones.

3.4.2 Effects of decay on furfurylated wood cell walls

When comparing the CLSM images of the furfurylated wood specimens before and after decay (42 weeks) (Fig. 5), it can be seen that for both excitation wavelengths, fluorescence is missing from regions of the cell walls where signs of fungal activity are seen, most likely because wood

material simply is lost (compare Fig. 5D with 5E-F). When comparing furan polymer filled tracheid lumina, fluorescence appears to be somewhat weaker from regions bordering to cell walls where signs of fungal activity are seen (Fig. 5E-F). However, when comparing the three fluorophore populations identified in the specimens by use of MCR-ALS modelling (Fig. 6), no striking qualitative differences are seen. That is, largely the same populations seem to be present before and after decay, and in the same locations within the wood structure. A minor difference is seen in the distribution of the fluorophores to the model components, where components 2 and 3 appear to be somewhat mixed for the model of the undecayed specimen compared to what is seen for the decayed sample. Similar, but not identical, results were seen for the other data sets (results not shown).

4. Discussion

Although the results of this study show that both modifications are to some extent susceptible to brown rot degradation, it is important to keep in mind that these results are not necessarily reflecting real life in-service performance. The experiments were performed on small earlywood samples of *P. radiata*, homogeneously treated, exposed to an aggressive brown rot fungus under optimal growth conditions and with longer incubation time than in standard tests. Previous studies have shown that both modifications perform well in long term field trials (Larsson-Brelid and Westin, 2010; Westin, 2012). Durability assessment of a material, and the ranking between materials cannot be based on one single test as the performance varies depending on the test fungus, exposure time, climate, and type of decay test. If the aim is to understand how and why fungi degrade a wood material, or fails to degrade it, methods different from the current standard tests can give additional information, as explored here. The novelty of the study is to follow the decay rate in more detail for a prolonged test period using diverse methods to analyze the fungal mode of action.

For the acetylated wood, the IR results confirmed earlier studies reporting that deacetylation takes place during fungal decay (Fig. 3 and 4). Raman microspectroscopy could however not confirm these findings, nor locate the deacetylation to specific regions of the cell wall (Table 1). This may be because the most extensively degraded tissue were very fragile, and therefore not well represented in the samples prepared for Raman analyses. Thus, the Raman data are mostly representative for the less degraded regions, even for the degraded specimens. For Raman analyses, the most suitable solution would be to embed such fragile samples in polyethylene glycol before microtoming, and remove this embedment substance prior to Raman microspectroscopy, as suggested by Gierlinger et al. (2012).The light microscopy specimens were preserved in resin prior to microtoming and successfully showed many encapsulated fungal hyphae in the acetylated sample at the 28-week harvest time (Fig. 2H and

K). Encapsulation of hyphae may come from the fungus' ability to produce an extracellular sheath during the decomposition processes when exposed to stress (Vesentini et al. 2005). We used a carbohydrate specific staining (Periodic acid – Schiff's stain), which visualized presence of a polysaccharides and lignin in cell walls and fungal hyphae (Fig. 2G, and 2J-L). Both staining methods indicated presence of a hyphal sheath consisting of both carbohydrates and polyphenolics covering the hyphae in unmodified and acetylated wood (Fig. 2J, K). Such a sheath may enable attachment to the tracheid wall in order to facilitate degradation, as well as cover and protect the hyphae in a changing environment.

In contrast to the acetylated wood cell wall chemistry, the furan polymer within the cell walls of the furfurylated wood appeared to be largely unaffected by aggressive *R. placenta* decay after 42 weeks, at least with regards to its fluorescence properties. This suggests that the limited fungal decay (mass loss of about 15%) that took place in the beginning of the experiment (Fig. 1 and 2) did not involve alteration of the polymer, but loss of parts of it may have happened when the surrounding cell wall biopolymers were degraded (Fig. 5 and 6). The study thus confirms recent results by Ehmcke et al. (2020). Our hypothesis is that this 'threshold' of approximately 15% is reached when the fungus has utilized the accessible hemicellulose and cellulose components at the WPG used here and that what is left is protected by furfurylation modification. Based on Skrede et al. (2019) we know that furfurylation does not seem to influence the expression of core plant cell wall hydrolyzing enzymes, but the expression pattern was delayed and prolonged compared to unmodified wood. According to Beck et al. (2019), OH accessibility in furfurylated samples did not change with increasing WPGs. However, OH accessibility in furfurylated samples (mean WPG 32%) increased significantly after initiation of decay (approximately 1% mass loss), and then leveled out during the rest of the incubation period. This was attributed to initial degradation of crystalline cellulose regions and possible formation of new OH groups in lignin and the furfuryl alcohol polymer. Beck et al. (2019) suggested the formation of additional OH groups in furfuryl alcohol polymer may occur from hydroxyl radical cleavage of the ether bonds within the furan rings. The fluorescence landscapes in Figure 6 do not strengthen this hypothesis, i.e. the increase in OH accessibility does not seem to involve changes to the fluorescent parts of the furan polymer (Fig. 6).

For furfurylated wood, the mean mass loss over the period of weeks 18-42 was 13.6%. We have no measurements to document whether or not this was enough to affect strength properties. However, it is well known that for brown rot decay even low mass loss can result in significant strength loss. In the current study, the small size of the wood samples made it impossible to perform mechanical testing using the equipment available. While no directly relevant studies could be found in the literature, it is known that for sound furfurylated wood

modulus of elasticity (MOE) is not significantly changed compared to unmodified wood, while modulus of rupture (MOR) is slightly increased and impact bending strength is decreased (Lande et al., 2004; Epmeier et al., 2004). Winandy and Morrell (1993) found that for *R. placenta* decay of Douglas fir (*Pseudotsuga menziesii)*, a wood species with slightly higher density than Radiata pine, 12.2% mass loss resulted in 17.4% MOE loss. While these results are not directly comparable to furfurylated *Pinus radiata* subjected to fungal decomposition, they support the notion that some strength loss most likely took place for the furfurylated specimens studied here after the initial fungal decomposition. Based on this we believe the mass loss found cannot be dismissed as being without consequences for wood properties, and that the processes taking place during the initial phase of brown rot degradation of furfurylated wood are important to understand in spite of the fact that decomposition seems to stop after a few weeks.

The differences seen between the acetylated and furfurylated wood when exposed to brown rot decay indicate that a hypothetical lasting protection against fungal decay ideally should involve physical bulking of the wood cell wall by a polymer that is present throughout the structure and cannot be depolymerized by fungi, i.e. in essence an introduction of a “lignin 2.0”. Lignin has been found to protect cell wall carbohydrates mostly by reducing the access of fungal enzymes rather than by resulting in enzyme inactivation by nonproductive binding (Djajadi et al., 2018), which is interesting from a biomimicking perspective, and which strengthens the case for cell wall bulking. The current study gives rise to the speculation that solely relying on addition of chemical groups that bind to one or more of the existing biopolymers may be a risky modification strategy in the long run if the bond created is vulnerable to fungal bond breaking capabilities, such as for example the ether bond to acetyl groups.

It has been shown that moisture content *per se* plays an important role in wood protection (Thybring, 2013; Thybring et al., 2018). Consequently, consumption of hydroxyl groups in the modification process and thus a reduction in the number of free hydroxyl group left in the wood should in theory decrease vulnerability towards fungal decomposition by reducing the equilibrium moisture content (EMC) of modified wood. However, earlier studies have shown that the EMC does not seem to be linked to the number of accessible hydroxyl groups (Hill et al., 2005; Thybring et al., 2020; Yang et al., 2020). This is in agreement with the finding that furfurylated wood holds less water in ranges relevant to fungal decay (Thygesen et al., 2010b) and is more resistant to fungal degradation than unmodified wood (Westin, 2012) even though consumption of hydroxyl groups does not seem to take place during furfurylation (Barsberg

and Thygesen, 2017). The current study nevertheless shows that some degradation takes place initially in furfurylated wood, at least for the treatment level used here. Higher treatment levels can naturally be envisioned, but another aspect to consider in that case is that high-level modification with a polymer that does not bind to the wood cell wall may lead to microcracks being formed in the cell walls during the modification process. These cracks could in turn give rise to capillary condensation at high relative humidity levels (Thygesen et al., 2010b), which will be favorable for fungal decomposition.

In the current study, we used Radiata pine earlywood, i.e. wood samples with low natural durability, but on the other hand easy to impregnate homogeneously. If less permeable wood species are modified, gradients and poorly modified regions might easily occur, both on macro and on micro scale. For such species, we speculate that in practice these gradients would be much more important for durability than the detailed decomposition mechanisms studied here.

5. Conclusions

The study showed that while acetylated wood was eventually deacetylated during brown rot decay, the furan polymer formed within the wood cell wall seemed to remain unaffected after suffering an initial loss of material. This result indicates that while blocking of hydroxyl groups with acetyl groups gives transient wood protection, lasting protection by chemical modification requires bulking of the wood cell wall by a polymer not vulnerable to fungal depolymerization/removal. It should however be noted that both furfurylated and acetylated wood have earlier been found to have extensive durability in field tests, and that the present study was carried out on homogenously treated samples under conditions optimal for fungal decay and with a prolonged incubation time.

Acknowledgment

We thank Sigrun Kolstad for help with the fungal decay tests. This project was funded by The Research Council of Norway [grant 243663/E50 BioMim], NIBIO [PhD scholarship project no. 335006], Biotransformation [NIBIO funding grant no. 11077], The European Regional Development Fund Interreg Öresund-Kattegat-Skagerrak [grant number 20201851] and SNS Nordic Forest Research [grant number SNS-125].

References

Arantes, V., Goodell, B., 2014. Current understanding of brown-rot fungal biodegradation mechanisms: A Review, In: Nicholas, D.D., Goodell B., Schultz, T., (Eds.), Deterioration and Protection of Sustainable Biomaterials. ACS Series. Oxford University Press, pp. 3–21.

Barsberg, S., Thygesen, L.G., 2009. Poly(furfuryl alcohol) formation in neat furfuryl alcohol and in cymene studied by ATR-IR spectroscopy and density functional theory (B3LYP) prediction of vibrational bands. Vib. Spectrosc. 49(1), 52–63. https://doi.org/10.1016/j.vibspec.2008.04.013.

Barsberg, S.T., Thygesen, L.G., 2017. A combined theoretical and FT-IR spectroscopy study of a hybrid poly(furfuryl alcohol) - lignin material: Basic chemistry of a sustainable wood protection method. ChemistrySelect 2, 10818–10827. https://doi.org/10.1002/slct.201702104.

Beck, G., Hegnar, O.A., Fossdal, C.G., Alfredsen, G., 2018b. Acetylation of *Pinus radiata* delays hydrolytic depolymerisation by the brown-rot fungus *Rhodonia placenta*. Int. Biodeter. Biodegr. 135, 39–52. https://doi.org/10.1016/j.ibiod.2018.09.003.

Beck, G., Hill, C., Cocher, P.M., Alfredsen, G., 2019. Accessibility of hydroxyl groups in furfurylated wood at different weight percent gains and during *Rhodonia placenta* decay. Eur. J. Wood Wood Prod. 77, 953–955. https://doi.org/10.1007/s00lisbeth107-019-01445-4.

Beck, G., Thybring, E.E., Thygesen L.G., 2018a. Brown-rot fungal degradation and de-acetylation of acetylated wood. Int. Biodeter. Biodegr. 135, 62–70. https://doi.org/10.1016/j.ibiod.2018.09.009.

Beck, G., Thybring E.E., Thygesen, L.G., Hill, C., 2017. Characterization of moisture in acetylated and propionylated radiata pine using low-field nuclear magnetic resonance (LFNMR) relaxometry. Holzforschung 72, 225–233. https://doi.org/10.1515/hf-2017-0072.

Beleites, C., Sergo, V., Bonifacio, A., Dahms, M., Egert, B., Fuller, S., 2020. hyperSpec: Work with Hyperspectral Data, i.e. Spectra + Meta Information (Spatial, Time, Concentration). Cited 27. August 2020, online at https://CRAN.R-project.org/package=hyperSpec.

CEN, 1997. Wood preservatives. Accelerated ageing of treated wood prior to biological testing. Leaching procedure. CEN-EN 84. European Committee for Standardization (CEN), Brussels, Belgium.

CEN, 2001. Wood preservatives. Determination of the effectiveness against soft rotting micro-fungi and other soil inhabiting micro-organisms. CEN-ENV 807. European Committee for Standardization (CEN), Brussels, Belgium.

572 Clausen, C.M., Kartal, N., 2003. Accelerated detection of brown-rot decay: Comparison of soil-
573 block test, chemical analysis, mechanical properties, and immunodetection. Forest
574 Prod. J. 53(11/12):90-94.

575 Curling, S., Clausen, C.A., Winandy, J.E., 2002. Relationships between mechanical properties,
576 weight loss, and chemical composition of wood during brown rot decay. For. Prod. J.,
577 52, 34–39.

578 del Cerro, M., Cogen, J., del Cerro, C., 1980. Stevenel's blue, an excellent stain for optical
579 microscopical study of plastic embedded tissues. Microsc. Acta 83, 117–121.

580 Djajadi, D.T., Jensen, M.M., Oliveira, M., Jensen, A., Thygesen, L.G., Pinelo, M., Glasius, M.,
581 Jorgensen, H., Meyer, A.S., 2018. Lignin from hydrothermally pretreated grass biomass
582 retards enzymatic cellulose degradation by acting as a physical barrier rather than by
583 inducing nonproductive adsorption of enzymes. Biotechnol. Biofuels 11, 85.
584 https://doi.org/10.1186/s13068-018-1085-0.

585 Ehmcke, G., Koch, G., Richter, K., Pilgard, A., 2020. Topochemical and light microscopic
586 investigations of non-enzymatic oxidative changes at the initial decay stage of furfuryl
587 alcohol-modified radiata pine (*Pinus radiata*) degraded by the brown rot fungus
588 *Rhodonia placenta*. Int. Biodeter. Biodegr. 154.
589 https://doi.org/10.1016/j.ibiod.2020.105020.

590 Eilers, P.H.C., Boelens, H.F.M., 2005. Baseline correction with asymmetric least squares
591 smoothing, Leiden University Medical Centre report, 2005.

592 Epmeier, H., Westin, M., Rapp, A., 2004. Differently modified wood: comparison of some
593 selected properties. Scand. J. For. Res. 19(5), 31–37.
594 https://doi.org/10.1080/02827580410017825.

595 Fackler, K., Stevanic, J.S., Ters, T., Hinterstoisser, B., Schwanninger, M., Salmén, L., 2010.
596 Localisation and characterisation of incipient brown-rot decay within spruce wood cell
597 walls using FT-IR imaging microscopy. Enzyme Microb. Technol. 47(6), 257–67.
598 https://doi.org/10.1016/j.enzmictec.2010.07.009.

599 Faix, O., 1991. Classification of lignins from different botanical origins by FT-IR spectroscopy.
600 Holzforschung 45(1), 21–8. https://doi.org/10.1515/hfsg.1991.45.s1.21.

601 Feder N., O'Brien T.P., 1968. Plant microtechnique: some principles and new methods. Am.
602 J. Bot. 55:123–142.

603 Fuchs, W., 1928. Zur Kenntnis des genuinen Lignins, In: Die Acetylierung des Fichtenholzes.
604 Berichte der deutschen chemischen Gesellschaft (A and B Series) 61(5), 948–951.
605 https://doi.org/10.1002/cber.19280610512.

606 Gierlinger, N., Keplinger, T., Harrington, M., 2012. Imaging of plant cell walls by confocal
607 Raman microscopy. Nat. Protoc. 7, 1694–1708.
608 https://doi.org/10.1038/nprot.2012.092.

609 Gierlinger, N., Schwanninger, M., 2007. The potential of Raman microscopy and Raman
610 imaging in plant research. Spectroscopy 21, 69–89.
611 https://doi.org/10.1155/2007/498206.

612 Goodell, B., Winandy. J.E., Morrell, J.J., 2020. Fungal degradation of wood: Emerging data,
613 new insights and changing perceptions. Coatings 2020, 10, 1210;
614 doi:10.3390/coatings10121210.

615 Hill, C.A.S., Forster, S.C., Farahani, M.R.M., Hale, M.D.C., Ormondroyd, G.A., Williams, G.R.,
616 2005. An investigation of cell wall micropore blocking as a possible mechanism for the
617 decay resistance of anhydride modified wood. Int. Biodeter. and Biodegr. 55, 69–76.
618 https://doi.org/10.1016/j.ibiod.2004.07.003.

619 Irbe, I., Andersons, B., Chirkova, J., Kallavus, U., Andersone, I., Faix, O., 2006. On the
620 changes of pinewood (*Pinus sylvestris* L.) Chemical composition and ultrastructure
621 during the attack by brown-rot fungi *Postia placenta* and *Coniophora puteana.* Int.
622 Biodeter. Biodegr. 57(2), 99–106.

623 Irbe, I., Andersone, I., Andersons, B., Noldt, G., Dizhbite, T., Kurnosova, N., Nupponen, M.,
624 Stewart, D. 2011. Characterisation of the initial degradation stage of Scots pine (*Pinus*
625 *sylvestris* L.) sapwood after attack by brown-rot fungus *Coniophora puteana*.
626 Biodegradation 22, 719–728. https://doi.org/10.1007/s10532-010-9449-6

627 Jaumot, J., de Juan, A., Tauler, R., 2015. MCR-ALS GUI 2.0: New features and applications.
628 Chemom. Intell. Lab. Syst. 140, 1-12. https://doi.org/10.1016/j.chemolab.2014.10.003.

629 Lande, S., Westin, M., Schneider, M., 2004. Properties of furfurylated wood. Scand. J. For.
630 Res. 19(Suppl 5), 22–30. https://doi.org/10.1080/0282758041001915.

631 Larsson-Brelid, P., Westin, M., 2010. Biological degradation of acetylated wood after 18 years
632 in ground contact and 10 years in marine water. IRG/WP 10-40522. The International
633 Research Group on Wood Preservation, Stockholm.

634 Marchessault, R.H., Liang, C.Y., 1962. Infrared spectra of crystalline polysaccharides. VIII.
635 Xylans. J. Polym. Sci. 59, 357–378. https://doi.org/10.1002/pol.1962.1205916813.

636 Mevik, B.-H., Wehrens, R., Liland, K.H., Hiemstra, P., 2020. pls: Partial Least Squares and
637 Principal Component Regression. Cited 27. August 2020. Online at https://CRAN.R-
638 project.org/package=pls.

639 Nordstierna, L., Lande, S., Westin, M., Karlsson, O., Furó, I., 2008. Towards novel wood-based
640 materials: chemical bonds between lignin-like model molecules and poly(furfuryl
641 alcohol) studied by NMR. Holzforschung 62, 709–713.
642 https://doi.org/10.1515/HF.2008.110.

643 Sandberg, D., Kutnar, A., Mantanis, G., 2017. Wood modification technologies - a review.
644 IForest - Biogeosciences and Forestry 10, 895-908. https://doi.org/10.3832/ifor2380-
645 010.

646 Schwanninger, M., Rodrigues, J.C., Pereira, H., Hinterstoisser, B., 2004. Effects of short-time
647 vibratory ball milling on the shape of FT-IR spectra of wood and cellulose.
648 Vib.Spectrosc. 36(1), 23–40. https://doi.org/10.1016/j.vibspec.2004.02.003.

649 Skrede, I., Solbakken, M.H., Hess, J., Fossdal, C.G., Hegnar, O., Alfredsen G., 2019. Wood
650 modification by furfuryl alcohol caused delayed decomposition response in *Rhodonia*
651 (*Postia*) *placenta*. Appl. Environ.l Microbiol. 85, e00338-19.
652 https://doi.org/10.1128/AEM.00338-19.

653 Thybring, E.E., 2013. The decay resistance of modified wood influenced by moisture
654 exclusion and swelling reduction. International Biodeterioration and Biodegradation
655 82, 87–95. https://doi.org/10.1016/j.ibiod.2013.02.004.

656 Thybring, E.E., Kymalainen, M., Rautkari, L., 2018. Moisture in modified wood and its
657 relevance for fungal decay. IForest - Biogeosciences and Forestry 11, 418–422.
658 https://doi.org/10.3832/ifor2406-011.

659 Thybring, E.E., Piqueras, S., Tarmian, A., Burgert, I., 2020. Water accessibility to hydroxyls
660 confined in solid wood cell walls. Cellulose 27, 5617–5627.
661 https://doi.org/10.1007/s10570-020-03182-x.

662 Thygesen, L.G., Barsberg, S., Venås, T.M., 2010a. The fluorescence characteristics of
663 furfurylated wood studied by fluorescence spectroscopy and confocal laser scanning
664 microscopy. Wood Sci. and Technol. 44, 51–65. https://doi.org/10.1007/s00226-009-
665 0255-4.

666 Thygesen, L.G., Ehmcke, G., Barsberg, S., Pilgård, A., 2020. Furfurylation result of Radiata
667 pine depends on the solvent. Wood Sci. .Technol. 54, 929–942.
668 https://doi.org/10.1007/s00226-020-01194-1.

669 Thygesen, L.G., Engelund, E.T., Hoffmeyer, P., 2010b. Water sorption in wood and modified
670 wood at high values of relative humidity. Part I: Results for untreated, acetylated, and
671 furfurylated Norway spruce. Holzforschung 6, 315–323.
672 https://doi.org/10.1515/hf.2010.044.

673 Vesentini, D., Dickinson. D.J., Murphy, R.J., 2005. The production of extracellular
674 mucilaginous material (ECMM) in two wood-rotting basidiomycetes is affected by
675 growth conditions. Mycologia 97, 1163–1170.
676 https://doi.org/10.1080/15572536.2006.11832726.

677 Westin, M., 2004. Furan polymer impregnated wood PCT/NO2003/000248 [WO 2004/011216
678 A2], 1–11. Patent.

679 Westin, M., 2012. Durability of furfurylated wood – results from laboratory and field tests in the
680 Ecobinders project. Proceedings of 43rd Annual Meeting of the International Research
681 Group on Wood Protection, Kuala Lumpur, Malaysia, IRG/WP 12-40602.

682 Wiley, J.H., Atalla, R.H., 1987. Band assignments in the raman spectra of celluloses.
683 Carbohydrate Research 160, 113-129. https://doi.org/10.1016/0008-6215(87)80306-3.

684 Winandy, J.E., Morrell, J.J., 1993. Relationship between incipient decay, strength, and
685 chemical composition of Douglas-fir heartwood. Wood Fiber Sci. 25(3), 278–288.
686 https://ir.library.oregonstate.edu/concern/articles/qz20ss911.

687 Winandy, J.E., 2016. Relating wood chemistry and strength. Part I. Wood structure and
688 chemistry. Pages 92-102 in SM LeVan-Green, ed. Proc. Soc. of Wood Science and
689 Technology (swst.org). Monona WI. 277 p.

690 Winandy, J.E. 2017. Relating wood chemistry and strength: Part II. Fundamental relationships
691 between changes in wood chemistry and strength of wood. Wood Fiber Sci. 47, 2–11.

692 Yang, T.T., Thybring, E.E., Fredriksson, M., Ma, E.N., Cao, J.Z., Digaitis, R., Thygesen, L.G.,
693 2020. Effects of changes in biopolymer composition on moisture in acetylated wood.
694 Forests 11(7), 719. https://doi.org/10.3390/f11070719.

695

Table 1. Summary of Raman results for acetylated samples. The table shows peak area ratios between the 1735 cm^{-1} band (carbonyl stretching) and respectively the aromatic ring stretching band at 1601 cm^{-1} assigned to lignin and the CH stretching band at 2894 cm^{-1} assigned to cell wall material. Mean peak area ratios (mean), standard deviation (SD) and the number of spectra included in the calculation are shown for spectra assigned to either the S2 cell wall layer (S2) or the middle lamella and the cell corners (ML and CC). No systematic differences were found between samples collected before and after fungal degradation, neither for S2 nor for ML/CC.

		Acetylation/lignin peak area ratio						Acetylation/cell wall peak area ratio					
		S2			ML and CC			S2			ML and CC		
Time	Image	mean	SD	n	mean	SD	n	mean	SD	n	mean	SD	n
0W	1	0.31	0.15	8548	0.16	0.09	1995	0.04	0.02	8548	0.04	0.03	1995
0W	2	0.29	0.15	5974	0.15	0.08	1489	0.03	0.01	5974	0.04	0.02	1489
0W	3	0.61	0.49	2608	0.52	0.44	2121	0.11	0.16	2608	0.30	0.35	2121
28W	4	0.25	0.14	2485	0.13	0.08	690	0.03	0.01	2485	0.06	0.03	690
28W	5	0.21	0.09	8799	0.12	0.05	2563	0.03	0.01	8799	0.03	0.01	2563
28W	6	0.44	0.43	2498	0.44	0.41	1639	0.07	0.12	2498	0.27	0.32	1639

Figure captions

Figure 1

Mass loss development during *Rhodonia placenta* decomposition of *Pinus radiata* wood modified using either furfurylation (WPG 37) or acetylation (WPG 21) and compared to unmodified wood. For practical purposes more than 30% mass loss is regarded as severe decay (failure). We consequently terminated the experiment for the acetylated samples after 28 weeks as 42.8% mass loss was reached at that point.

Figure 2

Light microscopy visualization of the differently modified *Pinus radiata* wood, as compared to wood without any modification and after different times of subjection to *Rhodonia placenta*. A, D: unmodified wood at start of the experiment (0) and after 4 weeks (W) of fungal degradation. B, E, G: Acetylated wood at 0, 2 and 28 weeks of fungal degradation, respectively. C, F, H: Furfurylated wood at 0, 3 and 42 weeks of fungal degradation, respectively. I, J, K, L: PAS carbohydrate specific staining of sections from un-modified (0 and 4 W), acetylated (28 W), and furfurylated (42 W) wood visualizing insoluble polysaccharides of wood and fungal cell walls magenta to purplish red. Black arrows indicate examples of fungal hyphae. Bars (A-L) = 50 µm.

Figure 3

FTIR spectra of unmodified, acetylated and furfurylated *Pinus radiata* prior to decay and after degradation by *Rhodonia placenta* for 4 weeks, 28 weeks and 42 weeks, respectively (A). Lines show average values from all replicates and shaded ribbons show ± one standard deviation. Note the broken x-axis between 2800-1900 cm^{-1}. Panel B shows a closer view of the same data, including only the undegraded samples.

Figure 4

Regression coefficients of PLS models of mass loss prediction from FTIR spectra for unmodified, acetylated and furfurfylated *Pinus radiata* degraded by *Rhodonia placenta*.

Figure 5

Example CLSM images of furfurylated *Pinus radiata* before (A-C) and after (D-F) 42 weeks of decay by *Rhodonia placenta.* A and D show pseudo light microscopy transmission images, B and E show color-coded emission intensity in the range 500-600 nm after excitation at 488 nm, and C and F show colour-coded emission intensity in the range 650-700 nm after excitation at 633 nm. For the color-coded images, the signal intensity scale goes from black over brown/red to white (grayscale in printed version: from black to white). Intensities are comparable between images obtained using the same excitation wavelength. The arrow in D points to one of several locations where cavities/hyphae are seen in the cell wall. Each image measures approximately 82 µm x 82 µm.

748 Figure 6

749 Results of MCR-ALS modelling of furfurylated wood based on 4-way CLSM data obtained
750 from the two regions seen in Figure 5. The left half of the figure concerns the undecayed
751 furfurylated specimen seen in Figure 5A-C, while the right half of the figure concerns the
752 decayed furfurylated specimen seen in Figure 5D-F. Figure 6 shows the three MCR-ALS
753 components of each of the two models: For the undecayed specimen, column 1 contains the
754 excitation-emission landscapes of the components, and column 2 shows qualitatively how
755 dominating they are in the model at different locations in the wood structure. For the decayed
756 specimen similar information is shown in columns 3 and 4. All color-coded signals go from
757 blue over green, orange to light yellow (grayscale in printed version: from black to white). The
758 color scales are individual to each panel.

759

Figure 1

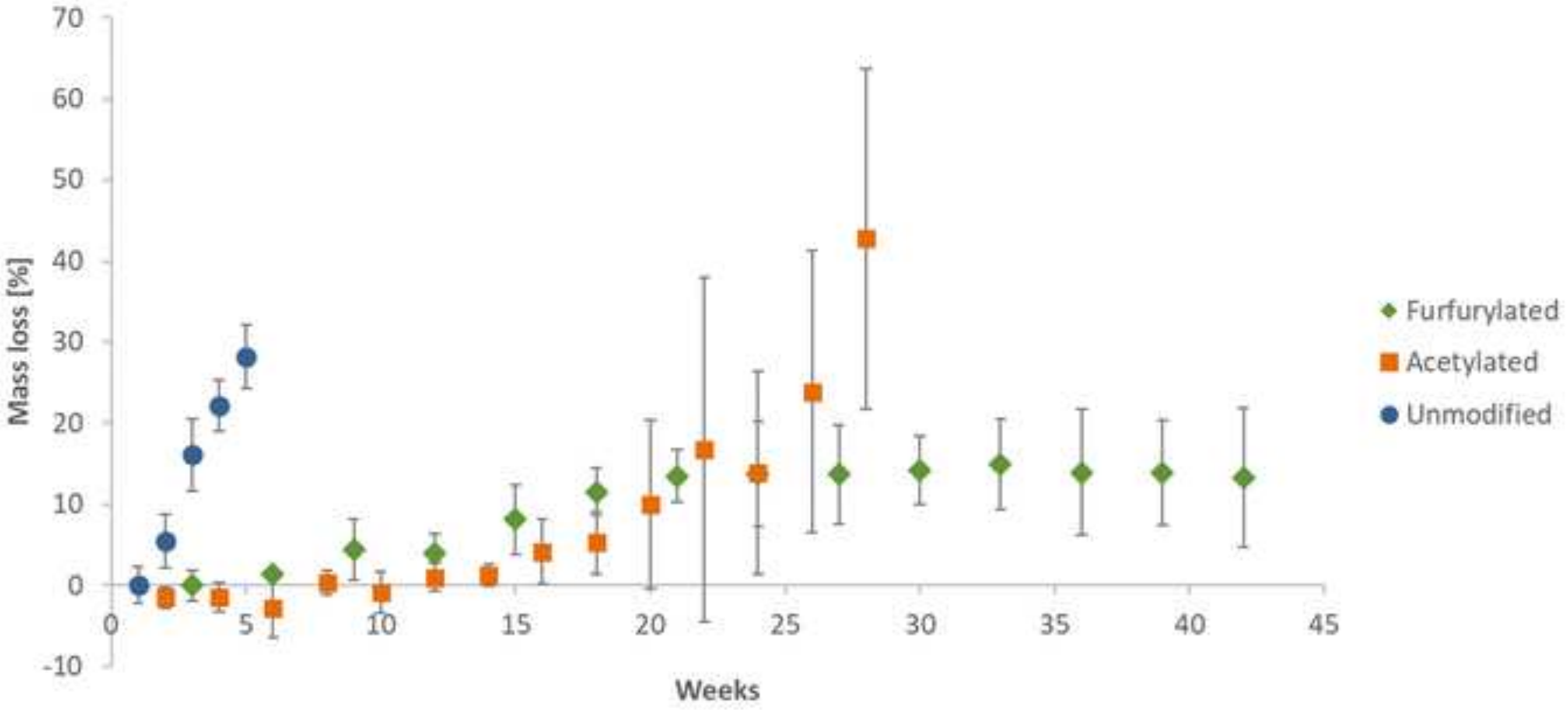

Figure 2

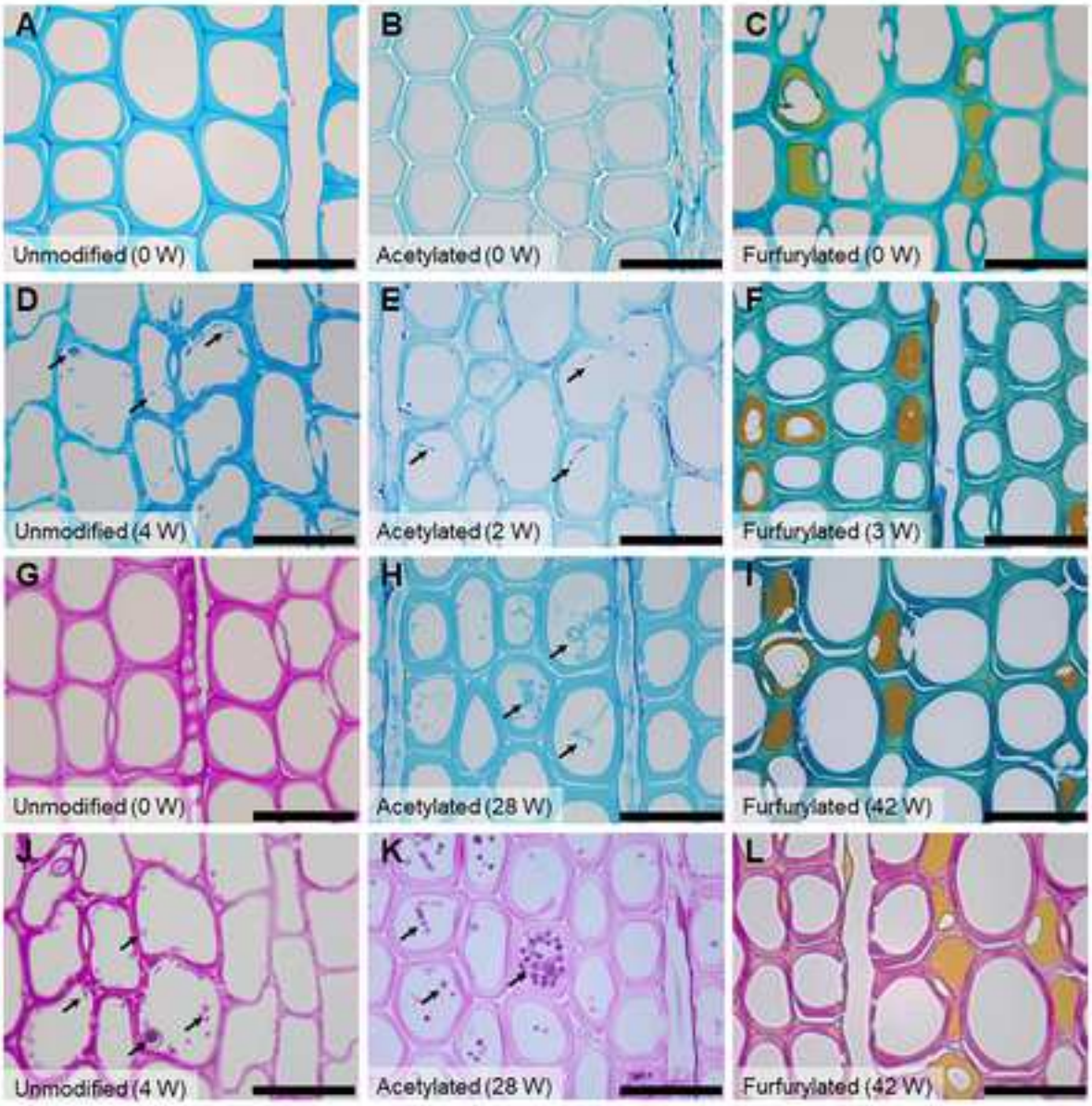

Figure 3

Click here to access/download;Figure;Fig3.tif

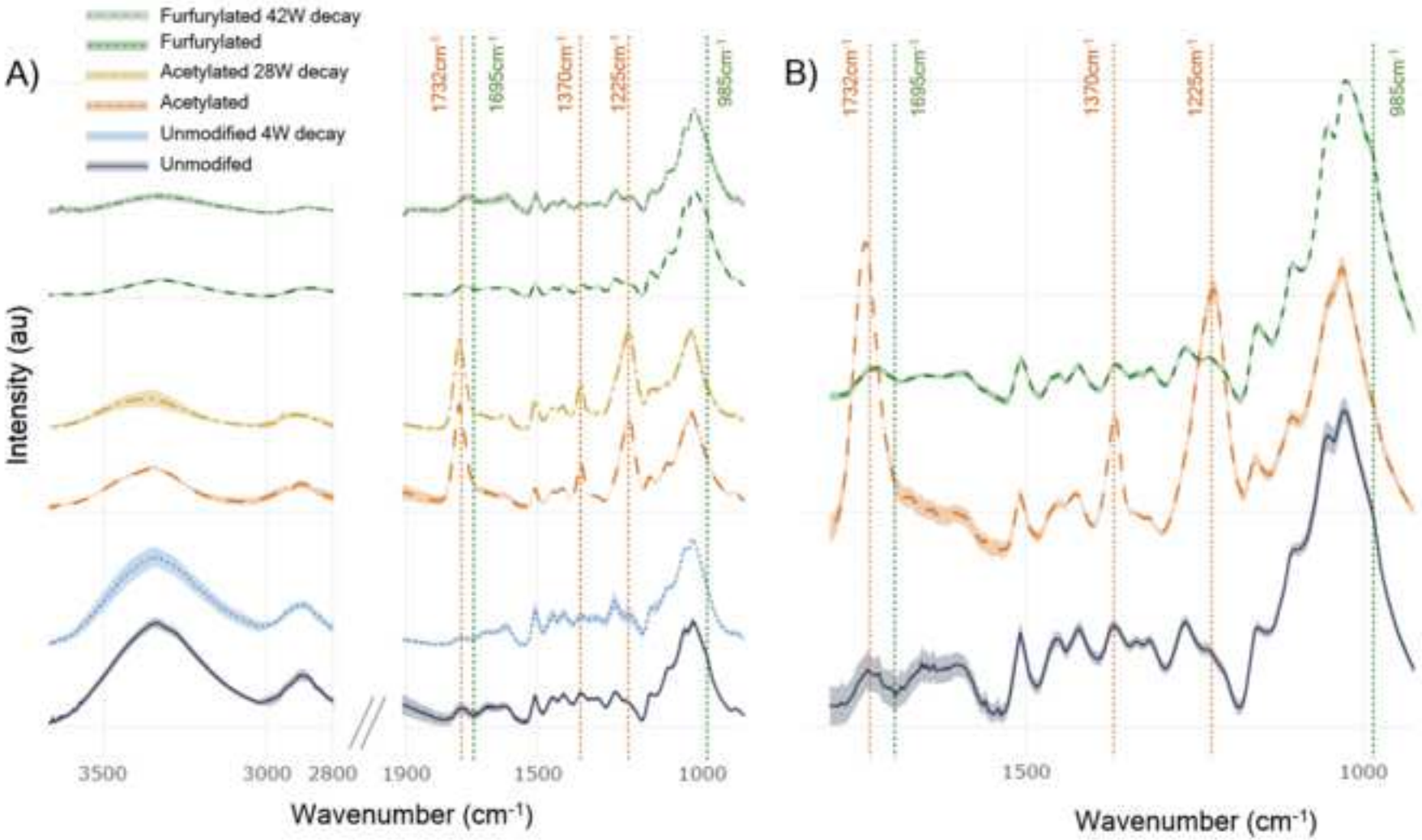

Figure 4

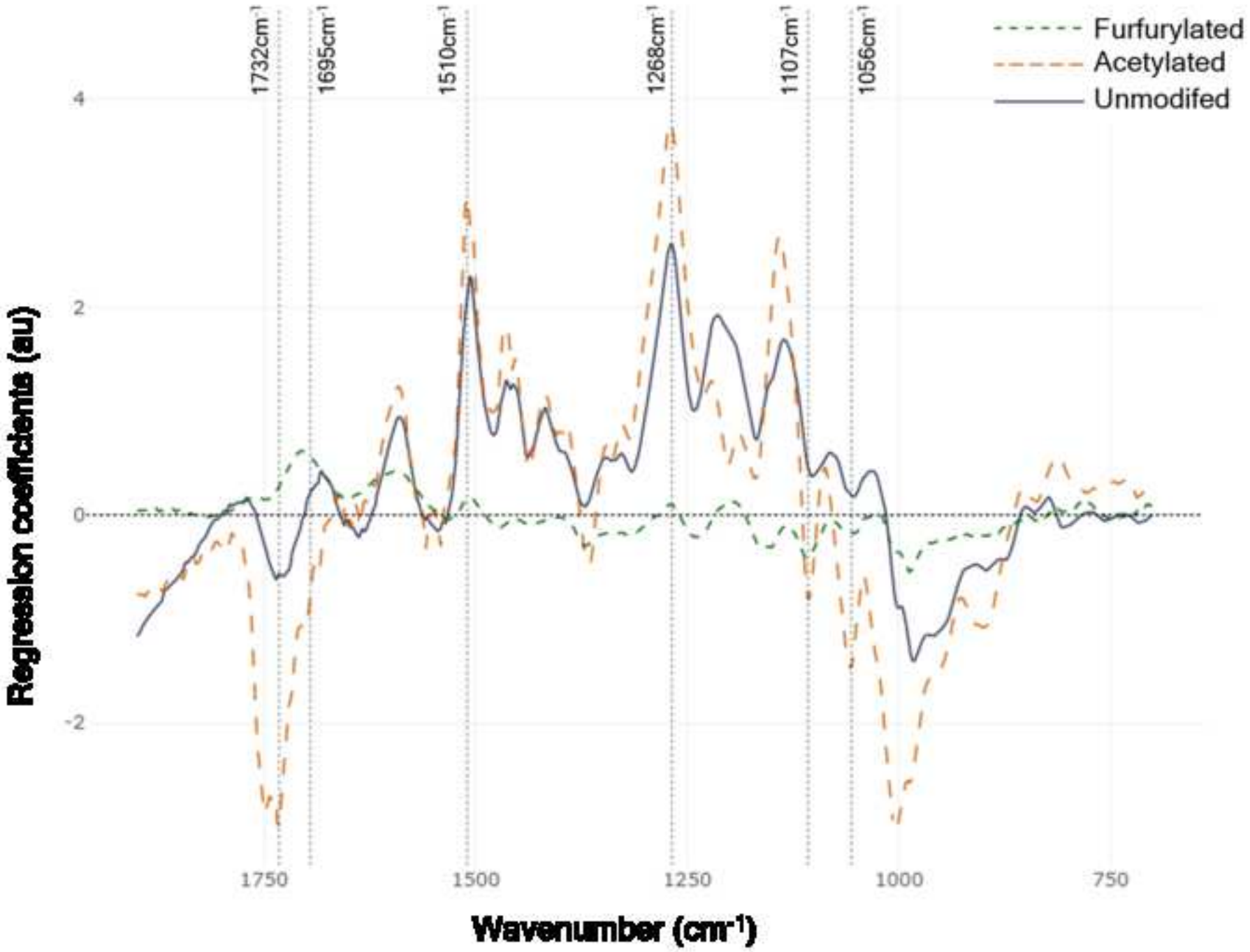

Figure 5

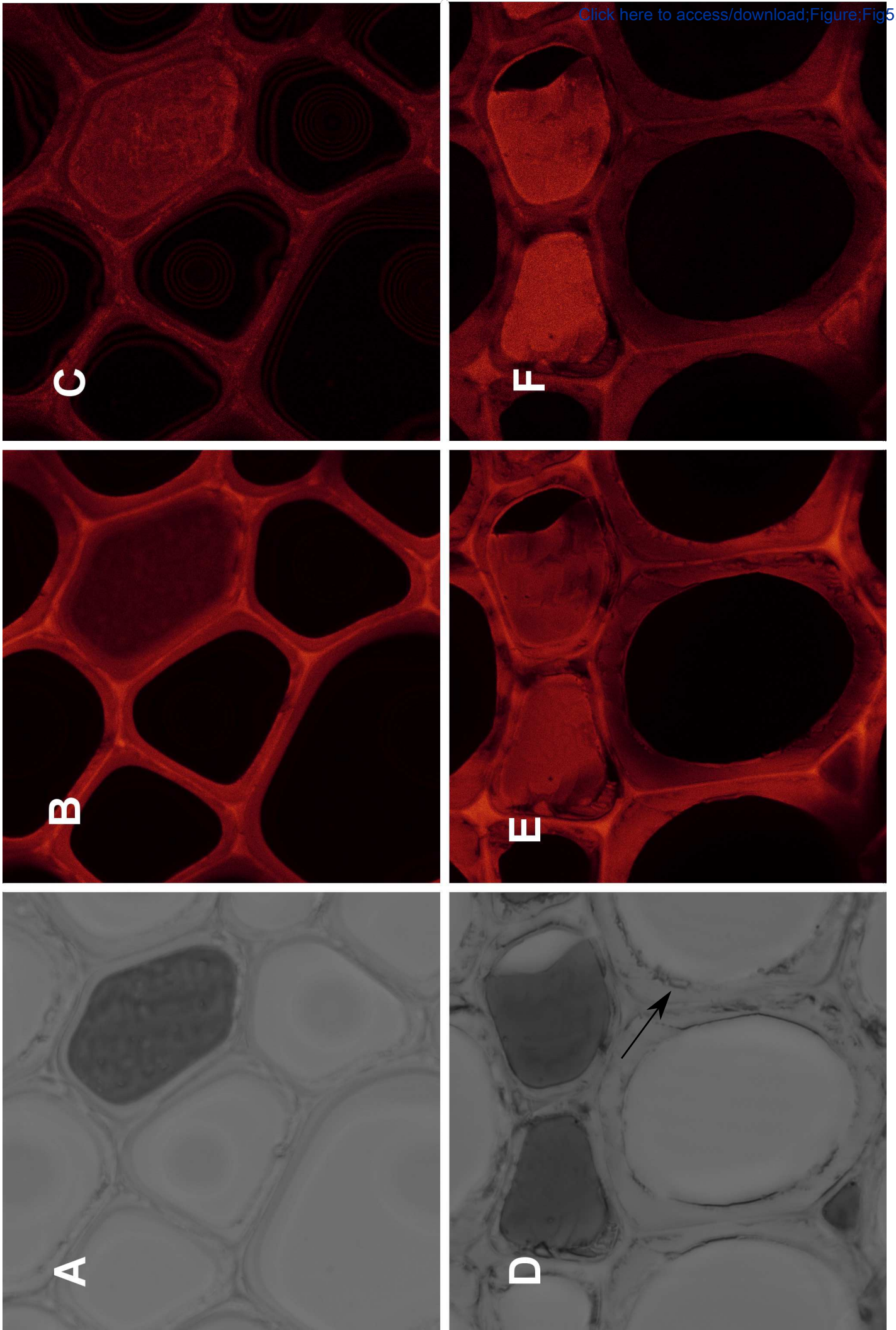

Figure 6

Click here to access/download;Figure;Fig6.tif

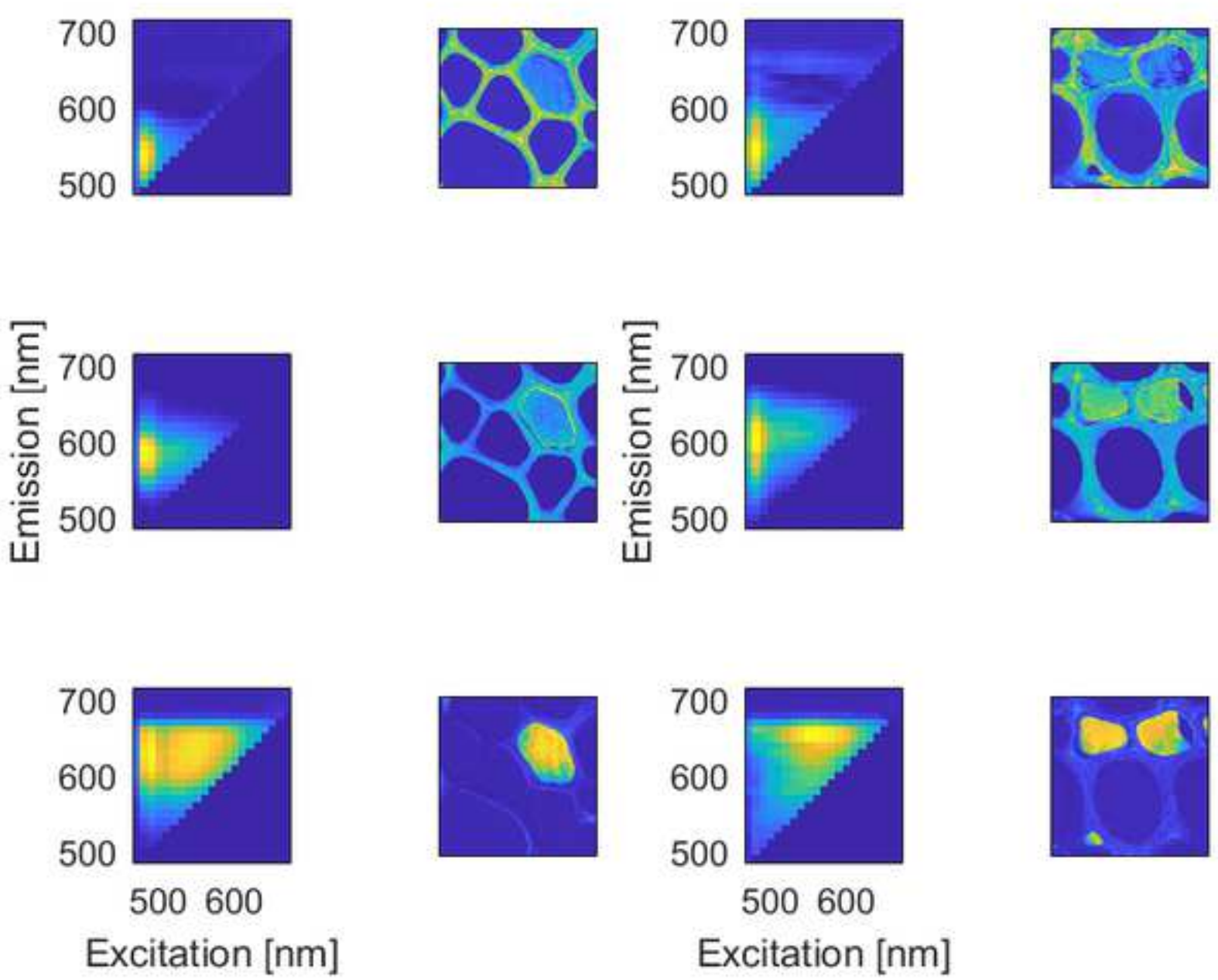

To the editor of IBB

The authors confirm that they have no conflicting interests.

Best regards,

Lisbeth G. Thygesen

(on behalf of all authors)